PHILOSOPHICAL TRANSACTIONS OF THE ROYAL SOCIETY A MATHEMATICAL, PHYSICAL & ENGINEERING SCIENCES

Coupling modes of gold trimer superstructures

Alison M. Funston, Timothy J. Davis, Carolina Novo and Paul Mulvaney

Phil. Trans. R. Soc. A 2011 **369**, 3472-3482
doi: 10.1098/rsta.2011.0012

PHILOSOPHICAL TRANSACTIONS OF THE ROYAL SOCIETY A

Phil. Trans. R. Soc. A (2011) **369**, 3472–3482
doi:10.1098/rsta.2011.0012

Coupling modes of gold trimer superstructures

By Alison M. Funston[1,*], Timothy J. Davis[2,*], Carolina Novo[1] and Paul Mulvaney[1]

[1]*School of Chemistry and Bio21 Institute, University of Melbourne, Parkville, Victoria, VIC 3010, Australia*
[2]*CSIRO Materials Science and Engineering, Clayton South, Victoria, VIC 3169, Australia*

An experimental and theoretical examination of the coupling modes within superstructures of gold nanorod trimers is presented. The experimentally determined spectrum of the nanorod trimers is reported and the modes are elucidated using an electrostatic eigenmode method based on the coupling of evanescent electric fields. The theory is able to reproduce the experimental spectrum well, and the nature of the modes and interactions are discussed.

Keywords: surface plasmon resonance; plasmon hybridization; plasmon coupling; trimer; eigenmode; gold nanorod

1. Introduction

The interaction of electromagnetic radiation with nanosized metal particles leads to a collective oscillation of the electron cloud, giving rise to a localized surface plasmon resonance. This phenomenon results in the concentration of electromagnetic energy at the particle surface, known as the near-field. The near-field electromagnetic enhancement is dependent upon the size and shape of the particle, with a larger degree of focusing occurring at sharp apexes of the particle. The close approach of two nanoparticles to within 2.5 times the particle diameter leads to a significant overlap of their electromagnetic near-fields, resulting in an interaction between their localized surface plasmon resonances. This interaction has been exploited in a number of applications, including surface-enhanced Raman spectroscopy (SERS) to allow the detection of single molecules [1–5], the universal plasmon ruler, which has been used to measure the distance between two metal nanoparticles in biological systems [6–9], and in optoelectronics, where the near-field coupling of nanoparticles spaced less than two diameters apart results in the transmission of light energy down a nanoparticle chain [10–14] or through an array [15], giving rise to waveguiding effects in which the energy is confined to sub-wavelength dimensions.

The near-field interaction between nanoparticles is highly distance-dependent and this distance dependence has been investigated extensively for pairs of spheres and discs, both lithographically fabricated, and for single crystals

*Authors for correspondence (alison.funston@monash.edu; tj.davis@csiro.au).

One contribution of 9 to a Theo Murphy Meeting Issue ‘Metallic metamaterials and plasmonics’.

[7,16–21]. More recently, it was determined that the degree of coupling between crystalline particles of lower symmetry (nanorods) is highly dependent on the geometry of the constituent particles [17]. The interaction between two particles has been modelled theoretically using a number of methods, including classical descriptions such as the discrete dipole approximation (DDA) [16], the boundary element method (BEM) [22], finite-difference time domain (FDTD) and multipole expansion methods [23]. These have recently been reviewed and compared [24] and the reader is directed to this review for more information. More recently, a quantum mechanical description has been developed, which has highlighted the importance of electromagnetic screening and electron tunnelling in the interparticle gap at very small particle separations [25].

For systems containing a larger number of particles with variable geometry, the modelling of the coupling becomes more difficult. One approach to circumvent this is to use the electrostatic approximation, which allows us to represent the interactions in terms of the natural plasmonic resonances (eigenmodes) of the metallic nanostructures. This representation makes the formalism applicable to arbitrary shapes and leads to relatively simple relationships for the coupling between nanostructures. Recently, we reported an extension of the work of Mayergoyz *et al.* [26] on the electrostatic resonances of nanoparticles, also known as the non-retarded BEM [27], to include the effects of interparticle coupling and radiation losses [28]. Simple analytical expressions for this model have been derived that enable us to estimate the resonant frequencies and modes in coupled systems of nanoparticles [29]. Here, we use this model to identify resonant modes associated with experimental optical spectra from trimers of nanorods in different geometries. Although the model is unable to predict the resonance wavelengths accurately at small interparticle separation, it is able to highlight the key features observed in the spectra.

2. Experimental procedures

The particles were chemically synthesized [30,31] and are single crystals. To correlate the geometry and size of the nanorods within the trimers and their scattering spectrum, we used a focused ion beam (FIB)-based registration method [32]. The rods were dispersed in indium tin oxide (ITO)-coated glass slides, and markers were etched in the substrate using an FIB [32]. The etched markers were located and imaged, and the scattering spectra of the particles around the markers were collected using a dark-field microscope. The microscope setup consisted of a 0.8–0.95 numerical aperture (NA) dry dark-field condenser and Nikon Plan Fluor ELWD 40×/0.60 NA objective coupled to a MicroSpec 2150i and Pixis 1024 Acton thermoelectrically cooled charge-coupled device (CCD) (Princeton Instruments). The excitation light in this setup was unpolarized. The scanning electron microscope (SEM) images of the same particles were also collected, allowing direct correlation of the size, shape and arrangement of the trimers with the scattering spectrum. The trimers were formed largely fortuitously when the rods were spin-coated onto the ITO; the vast majority of rods in the samples existed as separated, single crystals.

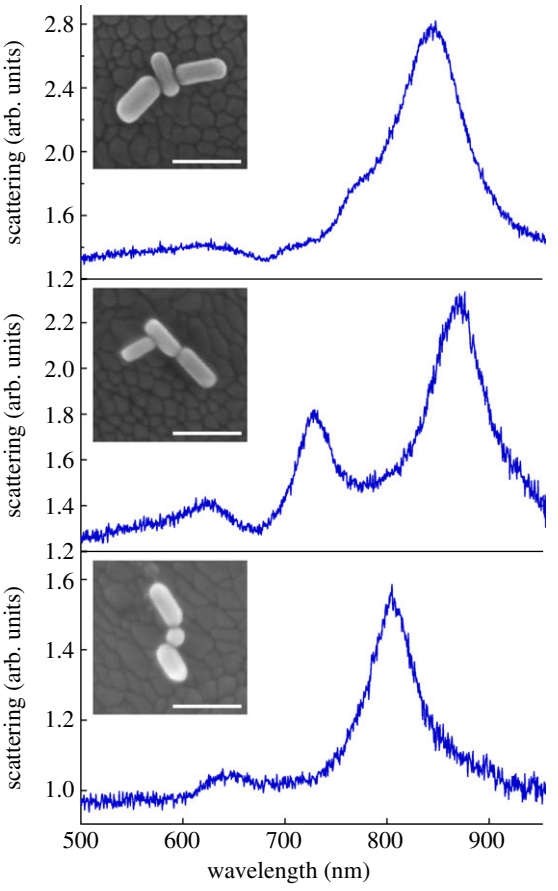

Figure 1. Scattering spectrum of gold nanorod trimers on ITO and in air. Insets show the SEM images of the particles giving rise to each scattering spectrum. Scale bar, 100 nm. (Online version in colour.)

3. Results and discussion

The scattering spectra and SEM images of gold nanocrystal trimers with the particles arranged in various configurations were collected and these are shown in figure 1. All these particles are arranged as close as possible to one another; from the SEM image, we estimate that this spacing is of the order of 1 nm, close to the resolution of the SEM image. The cetyl trimethylammonium bromide (CTAB) surfactant molecules coating the gold rods are 1.7 nm long [33]. A monolayer on each surface yields a separation of 3.5 nm, while complete interdigitation would lead to a separation of the order of 1–2 nm [33]. Within these trimers, the particles are interacting; however, the individual resonances of the three rods in the fully decoupled limit vary slightly due to small differences in aspect ratio. The individual rods shown in figure 1 have aspect ratios varying between 2.1 and 2.7, and their individual, uncoupled plasmon resonances are expected to vary between 624 and 678 nm [17].

The interaction between the three nanoparticles is analysed using the coupling theory of Davis *et al.* [28,29,34]. The theory represents the resonances in terms of surface-charge eigenfunctions that are excited by the electric field of the incident light (some examples of the eigenfunctions are shown later). The strength of the excitation is described by an excitation amplitude $a_q^j(\omega)$ for mode j of nanoparticle q. An approximate analytical expression for the excitation amplitude is

$$a_q^j(\omega) \approx -\frac{A_q^j \mathbf{p}_q^j . \mathbf{E}_0(\omega)}{\omega - \omega_q^j + \mathrm{i}\Gamma_q^j/2}, \tag{3.1}$$

where $\mathbf{p}_q^j$ is proportional to the dipole moment of mode j of particle q, $\mathbf{E}_0(\omega)$ is the amplitude of the electric field vector associated with the incident light, which is approximated as a constant over the nanoparticle, ω_q^j is the resonant frequency of the mode, Γ_q^j is the loss term in the Drude model for the metal electric permittivity and A_q^j is a constant. For convenience, we write the resonance frequency and the loss term as $\Omega_p^j = \omega_q^j - \mathrm{i}\Gamma_q^j/2$. When this nanoparticle is placed in an ensemble of N nanoparticles, the excitation amplitudes are affected by the evanescent electric fields from the nearby nanoparticles. The modified excitation amplitude $\tilde{a}_p^k$ of the nanoparticle in the ensemble can be expressed in terms of the excitation amplitudes of the isolated nanoparticles by

$$\tilde{a}_p^k(\omega) = \sum_q \sum_j (\delta_{pq}\delta^{kj} - C_{pq}^{kj}(\omega))^{-1} a_q^j(\omega). \tag{3.2}$$

This equation can be thought of in terms of the inverse of a matrix involving coupling coefficients $C_{pq}^{kj}(\omega)$. In the situation we analyse here, we consider only one dominant resonant mode for each nanoparticle and we will drop the mode index. Specifically, for three coupled nanoparticles each exhibiting one dominant resonance, equation (3.2) can be written as

$$\begin{bmatrix} \tilde{a}_1 \\ \tilde{a}_2 \\ \tilde{a}_3 \end{bmatrix} = \begin{bmatrix} 1 & -C_{12} & -C_{13} \\ -C_{21} & 1 & -C_{23} \\ -C_{31} & -C_{32} & 1 \end{bmatrix}^{-1} \begin{bmatrix} a_1 \\ a_2 \\ a_3 \end{bmatrix}. \tag{3.3}$$

This equation requires the inverse of a 3×3 matrix [35], which is straightforward. The resulting equation linking the excitations of each nanoparticle when isolated to the excitations when coupled is

$$\begin{bmatrix} \tilde{a}_1 \\ \tilde{a}_2 \\ \tilde{a}_3 \end{bmatrix} = \frac{1}{\Delta_3} \begin{bmatrix} 1 - C_{23}C_{32} & C_{12} + C_{13}C_{32} & C_{13} + C_{12}C_{23} \\ C_{21} + C_{23}C_{31} & 1 - C_{13}C_{31} & C_{23} + C_{21}C_{13} \\ C_{31} + C_{32}C_{21} & C_{32} + C_{31}C_{12} & 1 - C_{12}C_{21} \end{bmatrix} \begin{bmatrix} a_1 \\ a_2 \\ a_3 \end{bmatrix}, \tag{3.4}$$

where $\Delta_3 = 1 - C_{12}C_{21} - C_{13}C_{31} - C_{23}C_{32} - C_{12}C_{23}C_{31} - C_{13}C_{32}C_{21}$ is the three-particle determinant of the matrix inverse. Note that the excitation amplitudes in the ensemble become large when the real part of the determinant is zero, $\mathrm{Re}\,\Delta_3 = 0$. This is the condition for a resonance in the coupled system.

The coupling coefficient C_{pq}^{kj} determines the effect of the evanescent field from mode j of particle q on the resonance of mode k of particle p. This can be put in the form [29]

$$C_{pq}^{kj} \approx -\frac{G_{pq}^{kj}}{(\omega - \Omega_p^k)}, \tag{3.5}$$

where the geometric coupling term G_{pq}^{kj} is related to the electric field from particle q as determined by Coulomb's law. Here, we define $G_{pp}^{kj} = 0$. The geometric coupling depends on the distribution of the surface charges associated with the resonant mode of the nanoparticle and the effect of the electric field from these charges on the neighbouring nanoparticle. To the lowest order, it can be expressed in terms of the dipole moments of the modes [29]

$$G_{pq}^{kj} \approx \frac{A_p^k}{4\pi\epsilon_b d_{pq}^3}(3(\mathbf{p}_p^k \cdot \hat{\mathbf{d}}_{pq})(\mathbf{p}_q^j \cdot \hat{\mathbf{d}}_{pq}) - \mathbf{p}_p^k \cdot \mathbf{p}_q^j), \tag{3.6}$$

where $\hat{\mathbf{d}}_{pq}$ is the unit vector from the centre of the nanoparticle q to the centre of the nanoparticle p and d_{pq} is the distance. The electric permittivity of the background medium is ϵ_b. Equation (3.6) is useful in estimating the relative signs of the geometric coupling terms. It can be seen that, in this approximation, the coupling is symmetric, $G_{pq}^{kj} = G_{qp}^{jk}$. However, to understand the general behaviour of the coupling, we can often leave G_{pq}^{kj} as an unknown parameter.

The trimer geometries we analyse in this paper are shown in figure 2, where the three particles lie in the same plane. These are representations of the trimers observed experimentally, as shown in figure 1. The arrows on the nanoparticles indicate the directions of the dipole moments. This is useful in determining the relative values of the excitation amplitudes a_q^j of the isolated nanoparticles, as required in equation (3.1), and it allows equation (3.6) to be used to estimate the relative magnitudes of the geometric coupling. Also shown in figure 2 is the angle ϕ that defines the direction of polarization of the incident electric field.

We first analyse the structure shown in figure 2*a*. We will assume that the nanoparticles are identical, with a resonance frequency Ω_R, and assume that nanoparticles 1 and 3 are not directly coupled, $G_{13} = G_{31} \approx 0$. The dominant coupling is $G_{12} = G_{21} = G_{32} = G_{23} = -G$, where $G > 0$ is a constant. The negative sign is consistent with equation (3.6). The determinant of the matrix inverse with these geometric coupling terms leads to the equation

$$(\omega - \Omega_\mathrm{R} + \sqrt{2}G)(\omega - \Omega_\mathrm{R} - \sqrt{2}G) = 0.$$

This demonstrates two modes: one mode has a higher frequency (larger energy) than the individual nanoparticles and the other a lower frequency. There is a third resonance related to the uncoupled nanoparticles given by $(\omega - \Omega_\mathrm{R}) = 0$. The resonant modes corresponding to these frequencies have been calculated using a numerical solution to the electrostatic eigenvalue problem [26,28] and are also shown in figure 3*a* in order of increasing energy. If the nanoparticles 1 and 3 are tilted at an angle θ (see figure 2*a*), then the excitation amplitudes of the isolated nanoparticles are $a_1 = -a\cos(\theta - \phi)/(\omega - \Omega_\mathrm{R})$, $a_2 = -a\sin\phi/(\omega - \Omega_\mathrm{R})$ and $a_3 = a\cos(\theta + \phi)/(\omega - \Omega_\mathrm{R})$, where ϕ is the angle of the polarization vector of the

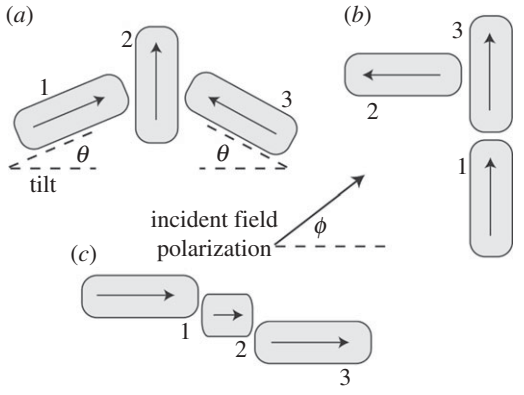

Figure 2. The trimer geometries that are analysed using the electrostatic model. These correspond to the configurations of figure 1. The arrows indicate the default directions of the dipole moments of the resonant modes that are used to estimate the relative excitation amplitudes and the Coulomb coupling. Also shown is the tilt angle θ of the nanoparticles in configuration (a) and the polarization angle ϕ of the incident field.

incident field (as shown in figure 2). Let $\delta\omega = \omega - \Omega_{\mathrm{R}}$. Then using equations (3.4) and (3.5) the excitation amplitudes of the coupled nanoparticle resonances are

$$\tilde{a}_1 = a\frac{(G^2 - \delta\omega^2)\cos(\theta - \phi) + G^2\cos(\theta + \phi) - G\delta\omega\sin\phi}{\delta\omega(\delta\omega - \sqrt{2}G)(\delta\omega + \sqrt{2}G)}, \tag{3.7}$$

$$\tilde{a}_2 = -a\frac{G\cos(\theta - \phi) - G\cos(\theta + \phi) + \delta\omega\sin\phi}{(\delta\omega - \sqrt{2}G)(\delta\omega + \sqrt{2}G)} \tag{3.8}$$

and

$$\tilde{a}_3 = -a\frac{(G^2 - \delta\omega^2)\cos(\theta + \phi) + G^2\cos(\theta - \phi) + G\delta\omega\sin\phi}{\delta\omega(\delta\omega - \sqrt{2}G)(\delta\omega + \sqrt{2}G)}. \tag{3.9}$$

The scattering spectrum is proportional to $|\mathbf{p}|^2$, which involves the total dipole moment $\mathbf{p} = \tilde{a}_1\mathbf{p}_1 + \tilde{a}_2\mathbf{p}_2 + \tilde{a}_3\mathbf{p}_3$, and this, in turn, depends on the individual dipole moments $\mathbf{p}_q$ of the modes of each nanoparticle. Here, we have assumed that the magnitudes are the same but they have different orientations, as shown in figure 2. The scattering spectrum calculated using equations (3.8)–(3.10) is shown in figure 3*a*. The polarization-averaged spectrum reproduces the experimental results for this arrangement as a single main resonance with some structure. The calculation depends on the coupling parameter G that relates to the Coulomb interaction between the surface charges associated with the localized surface plasmons. As derived above, this parameter controls the shift of the resonances according to $\omega = \Omega_{\mathrm{R}} \pm \sqrt{2}G$. The width of each resonance is determined by the internal losses in the nanoparticles, described by the Drude loss factor Γ. We have chosen G to be slightly smaller than Γ so that the calculated spectrum resembles that in figure 1. For light incident with $\phi = 90°$, all three particles are excited and the resonance mode is spread across the entire structure. There is, however, little coupling to the perpendicular rod (as oriented in figure 3*a*) upon excitation with light with $\phi = 0°$. A strongly coupled dark

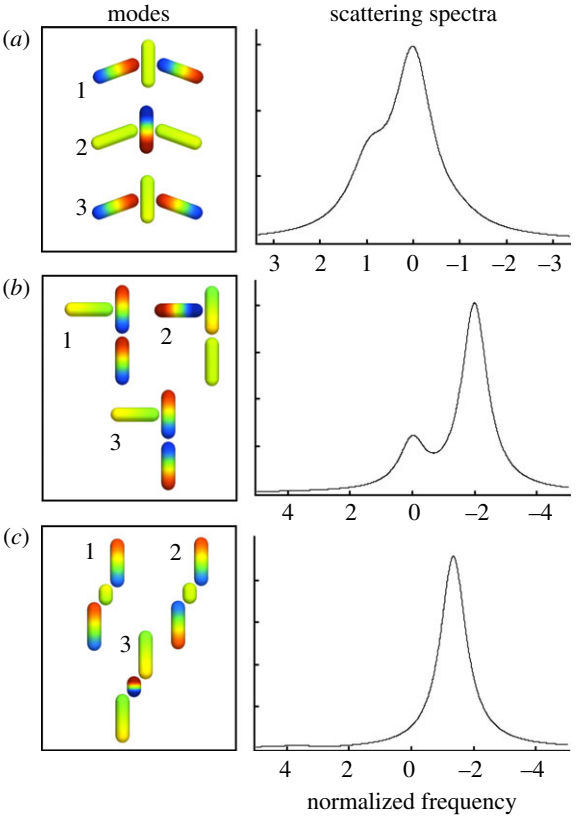

Figure 3. The modes associated with the coupled nanoparticles and the spectra calculated using the analytical formulae corresponding to the trimer configurations in figure 1. The frequency is in units of the loss parameter Γ with the origin set at ω_R for (a) and (b) and at $\omega_R - G_1$ for (c), and the spectra have been averaged over the incident light polarization. The modes were determined using a numerical solution to the eigenvalue problem [26,28]. The colour represents the strength of the localized surface plasmon resonance, with blue positive and red negative. The parameters used in calculating the spectra were: (a) $\theta = 20°$, $G/\Gamma = 0.67$, (b) $G/\Gamma = 2$ and (c) $G/\Gamma = 1.5$, $b/a = 0.5$, $\omega_H/\Gamma = 2$. (Online version in colour.)

mode is also predicted. This calculation compares well with the experimental data, particularly considering the approximations that have been used to derive the equations.

The structure in figure 2*b* has nanoparticle 2 perpendicular to nanoparticle 3. On the basis of the dipole formula (equation (3.6)), there is no coupling between them. This is not generally true because there will be coupling between the higher-order multipoles associated with the resonant modes. However, for our simple analysis we will take this coupling as small. Also, we will assume that nanoparticle 1 does not couple to nanoparticle 2 so that $G_{12} = G_{21} = G_{23} = G_{32} = 0$. Again, assuming that the nanoparticles are identical, with resonance frequency Ω_R, then the remaining coupling is $G_{13} = G_{31} = G$, where $G > 0$. The resonances of the coupled system are obtained, as before, from the determinant of the coupling matrix, leading to

$$(\omega - \Omega_R + G)(\omega - \Omega_R - G) = 0.$$

This shows a splitting of the resonances of nanoparticles 1 and 3. There is a third resonance given by $(\omega - \Omega_R) = 0$, which corresponds to the uncoupled second nanoparticle. The excitation amplitudes of the isolated nanoparticles are $a_1 = a_3 = -a\cos\phi/(\omega - \Omega_R)$ and $a_2 = a\sin\phi/(\omega - \Omega_R)$, so that the coupled amplitudes are given by

$$\tilde{a}_1 = \frac{-a\cos\phi}{(\omega - \Omega_R + G)}, \tag{3.10}$$

$$\tilde{a}_2 = \frac{a\sin\phi}{(\omega - \Omega_R)} \tag{3.11}$$

and

$$\tilde{a}_3 = \frac{-a\cos\phi}{(\omega - \Omega_R + G)}. \tag{3.12}$$

We note that the resonance with higher energy, $\omega = \Omega_R + G$, is not able to be excited in this system. That is, there is no excitation amplitude that has a maximum for this condition. This is a dark mode or subradiant mode. This is seen as mode 3 in figure 3*b*, which has opposing charge distributions on nanoparticles 1 and 3 and therefore has a zero dipole moment. If there was a coupling between nanoparticle 2 and the other nanoparticles, then we might expect that this mode could be excited. As before, the spectrum was calculated by adjusting the relative values of G and Γ to produce a spectrum that resembles that measured experimentally, as shown in figure 3*b*. The calculated spectrum gives two relatively strong resonances, one for light incident with polarization $\phi = 0°$ and one incident with polarization $\phi = 90°$. Two quite well-separated resonances are also observed experimentally. In each of these modes the coupling occurs only through two of the three rods, and is not transmitted to the third. This is in contrast to the case for the arrangement of figure 2*a* and is consistent with the findings for 'T' and 'L' structures for rod dimers [17]. From the results here, it is obvious that coupling occurring between a longitudinal mode and a transverse mode is not particularly strong, and excitation of the longitudinal mode of either rod does not lead to a significant transfer of this energy into the other rod. In geometries where the rods are all interacting via their longitudinal modes, the coupling is very strong and the plasmon resonance extends throughout the full structure. However, this is directional and only applicable for excitation of the perpendicular rod in the structure.

For the last structure, figure 2*c*, we have direct coupling between the two longer structures that we write as $G_{13} = G_{31} = G_l$ and the coupling to the smaller central nanoparticle (which is almost a sphere) is $G_{12} = G_{21} = G_{23} = G_{32} = G_s$ with $G_l > 0$ and $G_s > 0$. We assume that nanoparticles 1 and 3 are identical, with resonance Ω_R, but note that nanoparticle 2 is much smaller, with a higher resonance Ω_H. This means that the coupling coefficients are not symmetric. For example, $C_{12} = -G_s/(\omega - \Omega_R)$ whereas $C_{21} = -G_s/(\omega - \Omega_H)$. The determinant yields the three resonances

$$\omega = (\Omega_R + \Omega_H - G_l)/2 \pm \sqrt{8G_s^2 + (G_l + \Omega_H - \Omega_R)^2}/2$$

and $\omega = G_l + \Omega_R$. The excitation amplitudes are $a_1 = a_3 = -a/(\omega - \Omega_R)$ and $a_2 = -b/(\omega - \Omega_H)$, where we use two different constants, a and b, since the dipole moment of nanoparticle 2 is different from those of the other two nanoparticles.

The coupled amplitudes are then found to be

$$\tilde{a}_1 = \frac{a(\omega - \Omega_H) - G_s b}{2G_s^2 - (\omega - \Omega_R + G_l)(\omega - \Omega_H)}, \tag{3.13}$$

$$\tilde{a}_2 = \frac{b(\omega - \Omega_R + G_l) - 2G_s a}{2G_s^2 - (\omega - \Omega_R + G_l)(\omega - \Omega_H)} \tag{3.14}$$

and

$$\tilde{a}_3 = \frac{a(\omega - \Omega_H) - G_s b}{2G_s^2 - (\omega - \Omega_R + G_l)(\omega - \Omega_H)}. \tag{3.15}$$

The modes of the rod–sphere–rod trimer are essentially simple two-particle resonances due to the very small coupling between the sphere and the rods. Therefore, they should have the resonance of an equivalent two-rod system aligned end-to-end and this is borne out. A single intense peak with no structure is observed upon excitation with $\phi = 0°$ polarized light at 750–800 nm both experimentally and predicted via calculation. The spectrum shown in figure 3*c* shows the one dominant feature that arises from nanoparticles 1 and 3, which is the lower-frequency resonance. The higher-frequency resonance associated with the sphere (nanoparticle 3) has only a small dipole moment. A third resonance should occur at $\omega = G_l + \Omega_R$, but this resonance is absent in the expressions for the excitation amplitudes in equations (3.13) and (3.15). This situation arises because the mode is predominantly a quadrupole (mode 2 in figure 3*c*), which cannot couple with the incident light field.

In general, the analytical formulae show good qualitative agreement with the experimental data shown in figure 1. However, we must note that the calculated spectra are based on the assumption that only the fundamental dipole modes are involved in the coupling. Because of the very close proximity of the nanoparticles to one another, it is highly probable that higher-order modes will be excited and will contribute to the location of the resonances. Although the electrostatic dipole approximation used for these calculations breaks down at very small interparticle distances, we are interested in the modes and their relative energy levels rather than the absolute energy levels. The trends predicted by calculations all agree well with the experimental data. Indeed, it is only recently that quantum chemical calculations for two coupled particles have predicted the breakdown of classical theory at distances less than 1 nm [25], close to that observed here. In all the experimental data a very small resonance is observed around 600–650 nm. This is possibly a higher-order mode, such as a quadrupole mode, which is not predicted by the calculations due to the approximations used. It may also be due to the effects of symmetry breaking (as a result of the slightly different nanorod aspect ratios present in the assemblies) [36].

4. Conclusions

In summary, we have examined theoretically and experimentally the single-particle spectra of gold nanorod trimers. We find that the peaks can be identified and the relative intensities can be predicted using the plasmon coupling theory [28,29]. However, the precise plasmon energies depend upon an exact knowledge of particle morphology and spacing.

This work was supported through ARC DP grant 0451651 and FF grant 0561486. C.N. thanks the University of Melbourne for MIRS and MIFRS postgraduate scholarships. A.M.F. acknowledges support from a University of Melbourne Research Office Fellowship.

References

1 Kneipp, K., Wang, Y., Kneipp, H., Perelman, L. T., Itzkan, I., Dasari, R. R. & Feld, M. S. 1997 Single molecule detection using surface-enhanced Raman scattering (SERS). *Phys. Rev. Lett.* **78**, 1667–1670. (doi:10.1103/PhysRevLett.78.1667)

2 Kneipp, K., Kneipp, H. & Kneipp, J. 2006 Surface-enhanced Raman scattering in local optical fields of silver and gold nanoaggregates—from single-molecule Raman spectroscopy to ultrasensitive probing in live cells. *Acc. Chem. Res.* **39**, 443–450. (doi:10.1021/ar050107x)

3 Nie, S. & Emory, S. R. 1997 Probing single molecules and single nanoparticles by surface-enhanced Raman scattering. *Science* **275**, 1102–1106. (doi:10.1126/science.275.5303.1102)

4 Michaels, A. M., Jiang, J. & Brus, L. 2000 Ag nanocrystal junctions as the site for surface-enhanced Raman scattering of single rhodamine 6G molecules. *J. Phys. Chem. B* **104**, 11 965–11 971. (doi:10.1021/jp0025476)

5 Camden, J. P., Dieringer, J. A., Wang, Y., Masiello, D. J., Marks, L. D., Schatz, G. C. & Duyne, R. P. V. 2008 Probing the structure of single-molecule surface-enhanced Raman scattering hot spots. *J. Am. Chem. Soc.* **130**, 12 616–12 617. (doi:10.1021/ja8051427)

6 Reinhard, B. M., Siu, M., Agarwal, H., Alivisatos, A. P. & Liphardt, J. 2005 Calibration of dynamic molecular rulers based on plasmon coupling between gold nanoparticles. *Nano Lett.* **5**, 2246–2252. (doi:10.1021/nl051592s)

7 Jain, P. K., Huang, W. & El-Sayed, M. A. 2007 On the universal scaling behavior of the distance decay of plasmon coupling in metal nanoparticle pairs: a plasmon ruler equation. *Nano Lett.* **7**, 2080–2088. (doi:10.1021/nl071008a)

8 Sönnichsen, C., Reinhard, B. M., Liphardt, J. & Alivisatos, A. P. 2005 A molecular ruler based on plasmon coupling of single gold and silver nanoparticles. *Nat. Biotechnol.* **23**, 741–745. (doi:10.1038/nbt1100)

9 Reinhard, B. M., Sheikholeslami, S., Mastroianni, A., Alivisatos, A. P. & Liphardt, J. 2007 Use of plasmon coupling to reveal the dynamics of DNA bending and cleavage by single ECORV restriction enzymes. *Proc. Natl Acad. Sci. USA* **104**, 2667–2672. (doi:10.1073/pnas.0607826104)

10 Brongersma, M. L., Hartman, J. W. & Atwater, H. A. 2000 Electromagnetic energy transfer and switching in nanoparticle chain arrays below the diffraction limit. *Phys. Rev. B* **62**, R16 356–R16 359. (doi:10.1103/PhysRevB.62.R16356)

11 Maier, S. A., Brongersma, M. L., Kik, P. G., Meltzer, S., Requicha, A. A. G. & Atwater, H. A. 2001 Plasmonics—a route to nanoscale optical devices. *Adv. Mater.* **13**, 1501–1505. (doi:10.1002/1521-4095(200110)13:19<1501::AID-ADMA1501>3.0.CO;2-Z)

12 Maier, S. A., Kik, P. G., Atwater, H. A., Meltzer, S., Harel, E., Koel, B. E. & Requicha, A. A. G. 2003 Local detection of electromagnetic energy transport below the diffraction limit in metal nanoparticle plasmon waveguides. *Nat. Mater.* **2**, 229–232. (doi:10.1038/nmat852)

13 Krenn, J. R. *et al.* 1999 Squeezing the optical near-field zone by plasmon coupling of metallic nanoparticles. *Phys. Rev. Lett.* **82**, 2590–2593. (doi:10.1103/PhysRevLett.82.2590)

14 Quinten, M., Leitner, A., Krenn, J. R. & Aussenegg, F. R. 1998 Electromagnetic energy transport via linear chains of silver nanoparticles. *Opt. Lett.* **23**, 1331–1333. (doi:10.1364/OL.23.001331)

15 Maier, S. A., Friedman, M. D., Barclay, P. E. & Painter, O. 2005 Experimental demonstration of fiber-accessible metal nanoparticle plasmon waveguides for planar energy guiding and sensing. *Appl. Phys. Lett.* **86**, 071103. (doi:10.1063/1.1862340)

16 Gunnarsson, L., Rindzevicius, T., Prikulis, J., Kasemo, B., Käll, M., Zou, S. & Schatz, G. C. 2005 Confined plasmons in nanofabricated single silver particle pairs: experimental observations of strong interparticle interactions. *J. Phys. Chem. B* **109**, 1079–1087. (doi:10.1021/jp049084e)

17 Funston, A. M., Novo, C., Davis, T. J. & Mulvaney, P. 2009 Plasmon coupling of gold nanorods at short distances and in different geometries. *Nano Lett.* **9**, 1651–1658. (doi:10.1021/nl900034v)

18 Tamaru, H., Kuwata, H., Miyazaki, H. T. & Miyano, K. 2002 Resonant light scattering from individual Ag nanoparticles and particle pairs. *Appl. Phys. Lett.* **80**, 1826–1828. (doi:10.1063/1.1461072)

19 Marhaba, S., Bachelier, G., Bonnet, C., Broyer, M., Cottancin, E., Grillet, N., Lermé, J., Vialle, J.-L. & Pellarin, M. 2009 Surface plasmon resonance of single gold nanodimers near the conductive contact limit. *J. Phys. Chem. C* **113**, 4349–4356. (doi:10.1021/jp810405y)

20 Atay, T., Song, J.-H., Nurmikko, A. V. 2004 Strongly interacting plasmon nanoparticle pairs: from dipole–dipole interaction to conductively coupled regime. *Nano Lett.* **4**, 1627–1631. (doi:10.1021/nl049215n)

21 Rechberger, W., Hohenau, A., Leitner, A., Krenn, J. R., Lamprecht, B. & Aussenegg, F. R. 2003 Optical properties of two interacting gold nanoparticles. *Opt. Commun.* **220**, 137–141. (doi:10.1016/S0030-4018(03)01357-9)

22 Romero, I., Aizpurua, J., Bryant, G. W. & García de Abajo, F. J. 2006 Plasmons in nearly touching metallic nanoparticles: singular response in the limit of touching dimers. *Opt. Exp.* **14**, 9988–9999. (doi:10.1364/OE.14.009988)

23 Khlebtsov, B., Melnikov, A., Zharov, V. & Khlebtsov, N. 2006 Absorption and scattering of light by a dimer of metal nanospheres: comparison of dipole and multipole approaches. *Nanotechnol.* **17**, 1437–1445. (doi:10.1088/0957-4484/17/5/045)

24 Myroshnychenko, V., Rodriguez-Fernandez, J., Pastoriza-Santos, I., Funston, A. M., Novo, C., Mulvaney, P., Liz-Marzan, L. M. & García de Abajo, F. J. 2008 Modelling the optical response of gold nanoparticles. *Chem. Soc. Rev.* **37**, 1792–1805. (doi:10.1039/b711486a)

25 Zuloaga, J., Prodan, E. & Nordlander, P. 2009 Quantum description of the plasmon resonances of a nanoparticle dimer. *Nano Lett.* **9**, 887–891. (doi:10.1021/nl803811g)

26 Mayergoyz, I. D., Fredkin, D. R. & Zhang, Z. 2005 Electrostatic (plasmon) resonances in nanoparticles. *Phys. Rev. B* **72**, 155412. (doi:10.1103/PhysRevB.72.155412)

27 García de Abajo, F. J. & Howie, A. 2002 Retarded field calculation of electron energy loss in inhomogeneous dielectrics. *Phys. Rev. B* **65**, 115418. (doi:10.1103/PhysRevB.65.115418)

28 Davis, T. J., Vernon, K. C. & Gómez, D. E. 2009 Designing plasmonic systems using optical coupling between nanoparticles. *Phys. Rev. B* **79**, 155423. (doi:10.1103/PhysRevB.79.155423)

29 Davis, T. J., Gómez, D. E. & Vernon, K. C. 2010 Simple model for the hybridization of surface plasmon resonances in metallic nanoparticles. *Nano Lett.* **10**, 2618–2625. (doi:10.1021/nl101335z)

30 Nikoobakht, B. & El-Sayed, M. A. 2003 Preparation and growth mechanism of gold nanorods (NRs) using seed-mediated growth method. *Chem. Mater.* **15**, 1957–1962. (doi:10.1021/cm020732l)

31 Pérez-Juste, J., Liz-Marzán, L., Carnie, S., Chan, D. Y. C. & Mulvaney, P. 2004 Electric-field-directed growth of gold nanorods in aqueous surfactant solutions. *Adv. Funct. Mater.* **14**, 571–579. (doi:10.1002/adfm.200305068)

32 Novo, C., Funston, A. M., Pastoriza-Santos, I., Liz-Marzán, L. M. & Mulvaney, P. 2007 Spectroscopy and high-resolution microscopy of single nanocrystals by a focused ion beam registration method. *Angew. Chem. Int. Edn.* **46**, 3517–3520. (doi:10.1002/anie.200700033)

33 Biggs, S. & Mulvaney, P. 1994 Measurement of the forces between gold surfaces in water by atomic force microscopy. *J. Chem. Phys.* **100**, 8501–8505. (doi:10.1063/1.466748)

34 Gómez, D. E., Vernon, K. C. & Davis, T. J. 2010 Symmetry effects on the optical coupling between plasmonic nanoparticles with applications to hierarchical structures. *Phys. Rev. B* **81**, 075414. (doi:10.1103/PhysRevB.81.075414)

35 Davis, T. J., Vernon, K. C. & Gómez, D. E. 2009 Designing plasmonic systems: applications to dark modes in nanoparticle pairs and triplets. In *Plasmonics: Metallic Nanostructures and Their Optical Properties VII, San Diego, CA, 2–6 August*. Proc. SPIE, vol. 7394, 739423. Bellingham, WA: SPIE (doi:10.1117/12.825047)

36 Slaughter, L. S., Wu, Y., Willingham, B. A., Nordlander, P. & Link, S. 2010 Effects of symmetry breaking and conductive contact on the plasmon coupling in gold nanorod dimers. *ACS Nano* **4**, 4657–4666. (doi:10.1021/nn1011144)